Journal of Hazardous Materials 171 (2009) 431–435

Contents lists available at ScienceDirect

Journal of Hazardous Materials

journal homepage: www.elsevier.com/locate/jhazmat

$ZnFe_2O_4$ nanoparticles: Microwave-hydrothermal ionic liquid synthesis and photocatalytic property over phenol

Shao-Wen Cao[a,b], Ying-Jie Zhu[a,b,*], Guo-Feng Cheng[a], Yue-Hong Huang[a]

[a] State Key Laboratory of High Performance Ceramics and Superfine Microstructure, Shanghai Institute of Ceramics, Chinese Academy of Sciences, Shanghai 200050, PR China
[b] Graduate School of Chinese Academy of Sciences, PR China

ARTICLE INFO

Article history:
Received 14 January 2009
Received in revised form 13 April 2009
Accepted 5 June 2009
Available online 12 June 2009

Keywords:
Ionic liquid
Microwave-hydrothermal
Nanoparticles
$ZnFe_2O_4$
Phenol

ABSTRACT

We report the microwave-hydrothermal ionic liquid (MHIL) synthesis and photocatalytic property over phenol of $ZnFe_2O_4$ nanoparticles. $Zn(CH_3COO)_2{\cdot}2H_2O$ and $Fe(NO_3)_3{\cdot}9H_2O$ were used as the zinc and iron sources, respectively, in the presence of $CO(NH_2)_2$ and the ionic liquid 1-*n*-butyl-3-methyl imidazolium tetrafluoroborate ([BMIM][BF_4]). Deionized water was used as a solvent. The ionic liquid [BMIM][BF_4] and microwave heating temperature have significant influences on the crystal phase of the product. Different dosages of [BMIM][BF_4] or microwave heating temperature could lead to the formation of different products such as $ZnFe_2O_4$ and β-FeOOH. The MHIL method has the advantages such as simplicity, rapidness and energy saving. The $ZnFe_2O_4$ nanoparticles prepared by the MHIL method exhibit high photocatalytic activity for the degradation of phenol, which was up to 73% within 360 min. The TOC measurement confirmed the good photocatalytic efficiency of $ZnFe_2O_4$ nanoparticles.

© 2009 Elsevier B.V. All rights reserved.

1. Introduction

The fabrication of spinel-structured ferrite nanoparticles has been intensively investigated in recent years due to their unique physical and chemical properties, as well as technological applications in ferrofluids [1], high-density magnetic recording media [2], biomedicine [3], and radar-absorbent materials [4]. Particularly, zinc ferrite ($ZnFe_2O_4$) nanoparticles have aroused much interest owing to their potential applications in gas sensor and semiconductor photocatalysis because of their markedly different magnetic properties from those of their bulk counterpart [5]. It has been reported that $ZnFe_2O_4$ exhibits different properties with the change in particle size [6–10]. Several methods have been used for the preparation of $ZnFe_2O_4$ nanoparticles such as ball-milling technique, co-precipitation, aerogel and hydrothermal method [11–14]. However, some methods encounter problems such as the formation of the undesirable phase, the requirement of complicated equipment or time-consuming caused by multiple steps, etc. Therefore, it is intriguing to develop inexpensive, facile and fast methods for the preparation of single-phase zinc ferrite nanoparticles.

In recent years, the microwave-hydrothermal (MH) method has been rapidly developed due to rapid heating, faster kinetics, homogeneity, higher yield, better reproducibility, and energy saving compared with the conventional hydrothermal (CH) method [15–17]. Moreover, the MH method also enables chemical reactions to occur in the elevated-temperature and pressurized closed system in a short preparation time of minutes-level rather than days. Due to the excellent microwave absorbing ability, room temperature ionic liquids (RTILs) combined with microwave heating have been applied in nanomaterials synthesis [18–21]. The addition of a small quantity of an ionic liquid to a reaction solvent can greatly increase the heating rate. However, to the best of our knowledge, the synthesis of $ZnFe_2O_4$ nanoparticles by a microwave-hydrothermal ionic liquid (MHIL) method has not been reported.

Photocatalysis is a subject of current interest related to its application in effluent decontamination. Photocatalytic degradation of organic pollutants is becoming one of the most promising green chemistry technologies [22–24]. In most of the industries, phenolic compounds are widely used and have become common pollutants in waste water bodies. The phenolic compounds are quite stable and remain in the environment for a long period of time. Due to their toxicity and carcinogenic character, they are dangerous to the ecosystem in water bodies and human health [25]. A representative of this class of compounds is phenol. Sources of phenol include the process or waste solutions in chemical process industries, agriculture production, etc. [26,27]. Hence, the study on photocatalytic degradation of phenol in aqueous system is very important and significant.

* Corresponding author at: State Key Laboratory of High Performance Ceramics and Superfine Microstructure, Shanghai Institute of Ceramics, Chinese Academy of Sciences, 1295 Ding-Xi Road, Shanghai 200050, PR China. Tel.: +86 21 52412616; fax: +86 21 52413122.
E-mail address: y.j.zhu@mail.sic.ac.cn (Y.-J. Zhu).

0304-3894/$ – see front matter © 2009 Elsevier B.V. All rights reserved.
doi:10.1016/j.jhazmat.2009.06.019

In this work, we report the MHIL method for the preparation of $ZnFe_2O_4$ nanoparticles. The MHIL method has the advantages such as simplicity, rapidness and energy saving. The ionic liquid and reaction temperature have significant effects on the crystal phase of the product. Furthermore, $ZnFe_2O_4$ nanoparticles prepared by the MHIL method exhibit high photocatalytic activity for the degradation of phenol.

2. Materials and methods

2.1. Preparation of $ZnFe_2O_4$ nanoparticles

In a typical synthetic procedure, 0.110 g $Zn(CH_3COO)_2{\cdot}2H_2O$, 0.202 g $Fe(NO_3)_3{\cdot}9H_2O$, 0.08 g urea and 0.5 mL [BMIM][BF_4] were added into 25 mL deionized water under magnetic stirring. The resultant solution was loaded into a 60-mL Teflon autoclave, sealed, microwave-heated to 160 °C and kept at this temperature for 30 min. The microwave oven used for sample preparation was a microwave-hydrothermal synthesis system (MDS-6, Sineo, Shanghai, China). After cooled to room temperature, the product was collected and washed by centrifugation–redispersion cycles with deionized water. Please refer to Table 1 for the detailed preparation conditions for typical samples.

2.2. Photocatalytic activity measurements

The photocatalytic reactor consisted of two parts: a 70 mL quartz tube and a high-pressure Hg lamp. The Hg lamp was positioned parallel to the quartz tube. In all experiments, the photocatalytic reaction temperature was kept at about 35 °C. The reaction suspension was prepared by adding the sample (20 mg) into 50 mL of a phenol solution (20 mg L^{-1}). The suspension was sonicated for 15 min and then stirred in the dark for 30 min to ensure an adsorption/desorption equilibrium prior to UV irradiation. The suspension was then irradiated using UV light under continuous stirring. Analytical samples were taken out from the reaction suspension after various reaction times and centrifuged at 10,000 rpm for 5 min to remove the particles.

2.3. Characterization of samples

The prepared samples were characterized using X-ray powder diffraction (XRD, Rigaku D/max 2550 V, Cu Kα λ = 1.54178 Å), transmission electron microscopy (TEM, JEOL JEM-2100F), selected-area electron diffraction (SAED), high-resolution transmission electron microscopy (HRTEM) and energy dispersive spectroscopy (EDS). The photocatalytic reactions were carried out under irradiation of a 300 W high-pressure Hg lamp (GGZ300, Shanghai Yaming Lighting) with a maximum emission at about 365 nm. The phenol concentrations were analyzed using a UV–vis spectrophotometer (UV-2300, Techcomp) at a wavelength of 270 nm. The total organic carbon (TOC) was determined using a Vario EL Elemental Analyzer (Germany).

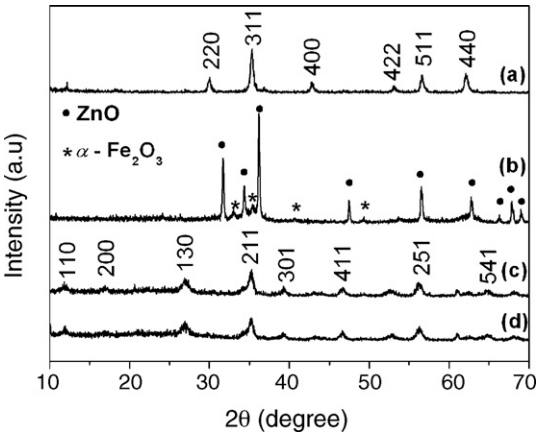

Fig. 1. XRD patterns of samples 1 (a), 2 (b), 3 (c), and 4 (d).

3. Results and discussion

The detailed preparation conditions and procedures for the samples are described in Section 2, and the preparation conditions for some typical samples are listed in Table 1.

Fig. 1a shows the XRD pattern of sample 1 prepared by MHIL method at 160 °C for 30 min, from which one can see that the product is a single phase of well-crystalline $ZnFe_2O_4$ with a spinel structure (JCPDS No. 73-1943). However, in the absence of ionic liquid ([BMIM][BF_4]), a mixture of ZnO and α-Fe_2O_3 (sample 2) is obtained, as shown in Fig. 1b. These results show that [BMIM][BF_4] has a significant effect on the crystal phase of the product, and [BMIM][BF_4] facilitates the formation of $ZnFe_2O_4$.

Fig. 2a shows TEM micrograph of $ZnFe_2O_4$ nanoparticles (sample 1). Fig. 2b shows a typical HRTEM micrograph with clear lattice fringes of an individual $ZnFe_2O_4$ nanoparticle (sample 1). The spacing d = 0.298 nm of fringes matches that of the (2 2 0) planes of spinel $ZnFe_2O_4$. The corresponding SAED pattern is shown in Fig. 2c. The nearest three spots in the SAED pattern can be indexed to (2 $\bar{2}$ 0), (4 0 0) and (2 2 0) planes of $ZnFe_2O_4$, which is consistent with the HRTEM observation. The corresponding EDS spectrum (Fig. 2d) confirms that the nanoparticle consists of Zn, Fe and O. The Cu peak is originated from the copper sample holder. Fig. 2e–g shows the HRTEM micrograph, the corresponding SAED pattern and EDS spectrum of another $ZnFe_2O_4$ individual nanoparticle (sample 1). The spacing d = 0.489 nm of fringes in Fig. 2f matches that of the (1 1 1) planes of spinel $ZnFe_2O_4$. The nearest three spots in the SAED pattern of Fig. 2f can be indexed to (1 1 $\bar{1}$), (2 2 0) and (1 1 1) planes of $ZnFe_2O_4$. The EDS spectrum (Fig. 2g) confirms that the nanopar-

Table 1
Experimental parameters for the preparation of typical samples by microwave-hydrothermal method at various temperatures for 30 min.

Sample no.	Solution	T [°C]	Product	pH
1	0.110 g $Zn(CH_3COO)_2{\cdot}2H_2O$ + 0.202 g $Fe(NO_3)_3{\cdot}9H_2O$ + 0.08 g $CO(NH_2)_2$ + 25 ml H_2O + 0.5 ml [BMIM]BF_4	160	$ZnFe_2O_4$	4.15
2	0.110 g $Zn(CH_3COO)_2{\cdot}2H_2O$ + 0.202 g $Fe(NO_3)_3{\cdot}9H_2O$ + 0.08 g $CO(NH_2)_2$ + 25 ml H_2O	160	ZnO + α-Fe_2O_3	6.57
3	0.110 g $Zn(CH_3COO)_2{\cdot}2H_2O$ + 0.202 g $Fe(NO_3)_3{\cdot}9H_2O$ + 0.08 g $CO(NH_2)_2$ + 25 ml H_2O + 1 ml [BMIM]BF_4	160	β-FeOOH	4.23
4	0.110 g $Zn(CH_3COO)_2{\cdot}2H_2O$ + 0.202 g $Fe(NO_3)_3{\cdot}9H_2O$ + 0.08 g $CO(NH_2)_2$ + 25 ml H_2O + 2 ml [BMIM]BF_4	160	β-FeOOH	4.01
5	0.110 g $Zn(CH_3COO)_2{\cdot}2H_2O$ + 0.202 g $Fe(NO_3)_3{\cdot}9H_2O$ + 0.08 g $CO(NH_2)_2$ + 25 ml H_2O + 0.5 ml [BMIM]BF_4	200	$ZnFe_2O_4$	4.04
6	0.110 g $Zn(CH_3COO)_2{\cdot}2H_2O$ + 0.202 g $Fe(NO_3)_3{\cdot}9H_2O$ + 0.08 g $CO(NH_2)_2$ + 25 ml H_2O + 0.5 ml [BMIM]BF_4	120	β-FeOOH	4.04
7	0.110 g $Zn(CH_3COO)_2{\cdot}2H_2O$ + 0.202 g $Fe(NO_3)_3{\cdot}9H_2O$ + 0.08 g $CO(NH_2)_2$ + 25 ml H_2O + 1 ml [BMIM]BF_4	120	β-FeOOH	3.70
8	0.110 g $Zn(CH_3COO)_2{\cdot}2H_2O$ + 0.202 g $Fe(NO_3)_3{\cdot}9H_2O$ + 0.08 g $CO(NH_2)_2$ + 25 ml H_2O + 2 ml [BMIM]BF_4	120	β-FeOOH	3.49

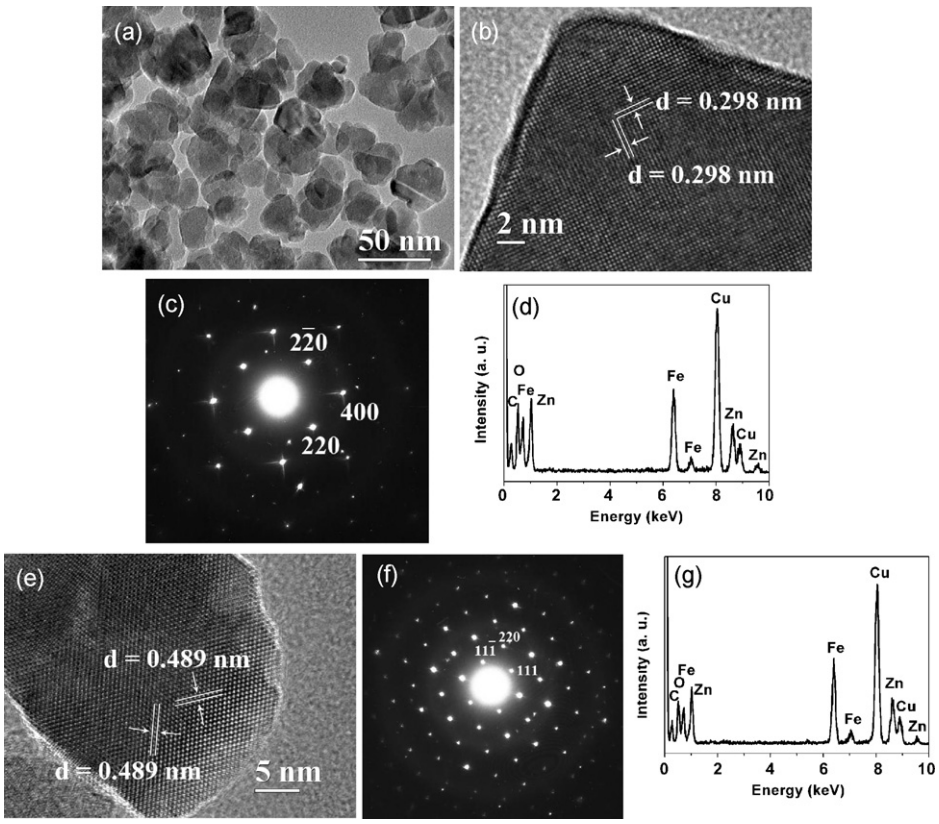

Fig. 2. TEM micrographs of sample 1 (a), HRTEM micrograph of an individual $ZnFe_2O_4$ nanoparticle (sample 1) (b) and its corresponding SAED pattern (c) and EDS spectrum (d), HRTEM micrograph of another individual $ZnFe_2O_4$ nanoparticle (sample 1) (e) and its corresponding SAED pattern (f) and EDS spectrum (g).

ticle consists of Zn, Fe and O. These experimental results indicate that well-crystalline $ZnFe_2O_4$ nanoparticles can be prepared by the MHIL method.

By controlling the dosage of $[BMIM][BF_4]$ added into the reaction solution, the crystal phase of the product can be controlled. As discussed above, in the absence of $[BMIM][BF_4]$ (Table 1, sample 2, Fig. 1b), a mixture of ZnO and α-Fe_2O_3 is obtained. When 0.5 mL of $[BMIM][BF_4]$ is added (Table 1, sample 1, Fig. 1a), the product is a single phase of $ZnFe_2O_4$. However, when the dosage of $[BMIM][BF_4]$ increases to 1 mL (Table 1, sample 3, Fig. 1c), the product is β-FeOOH (JCPDS No. 75-1594). Similar result to sample 3 is obtained when the dosage of $[BMIM][BF_4]$ is 2 mL (Table 1, sample 4, Fig. 1d). Therefore, the optimum dosage of $[BMIM][BF_4]$ for the production of $ZnFe_2O_4$ nanoparticles is 0.5 mL.

The microwave heating temperature also has a significant influence on the crystal phase of the final product. When the microwave heating temperature is 200 °C (Table 1, sample 5), the product still consists of $ZnFe_2O_4$ (Fig. 3a). However, when the microwave heating temperature is 120 °C (Table 1, sample 6), β-FeOOH is obtained (Fig. 3b). In addition, we also investigated the effects of different dosages of $[BMIM][BF_4]$ at 120 °C on the product. However, the product is still β-FeOOH when the dosage of $[BMIM][BF_4]$ is 1 or 2 mL (Table 1, samples 7 and 8, Fig. 3c and d). Therefore, the optimum temperatures for the production of $ZnFe_2O_4$ are above 160 °C.

A possible explanation for the formation of different products is proposed. In the solution, the zinc ion exists mainly as $[Zn(OH)_4]^{2-}$. The ionic liquid $[BMIM][BF_4]$ consists of cation $[BMIM]^+$ and anion $[BF_4]^-$, $[BMIM]^+$ can combine with $[Zn(OH)_4]^{2-}$ through the electrostatic interaction. The butyl group of $[BMIM]^+$ is hydrophobic. So the zinc ion locates in a relatively hydrophobic condition due to the coordination between $[Zn(OH)_4]^{2-}$ and $[BMIM]^+$. The relatively large size and hydrophobicity of $[BMIM]^+$ ions which are surrounding $[Zn(OH)_4]^{2-}$ make the hydrolyzation of zinc ions more difficult. So only the ferric ions hydrolyze to form β-FeOOH.

However, if the dosage of $[BMIM][BF_4]$ is not enough, the coordination between $[Zn(OH)_4]^{2-}$ and $[BMIM]^+$ is weakened at a high temperature. Hence, $ZnFe_2O_4$ forms by the co-precipitation of the zinc and ferric ions (samples 1 and 5).

In addition, we have measured the pH values of the final solutions after the preparation of all the above samples, and the results are listed in Table 1. One can see that in the absence of $[BMIM][BF_4]$ (sample 2), the pH value (6.57) is much higher than those of other solutions with the addition of $[BMIM][BF_4]$, indicating that the presence of $[BMIM][BF_4]$ significantly lowers the pH value of the reaction system. This may explain the formation of sample 2.

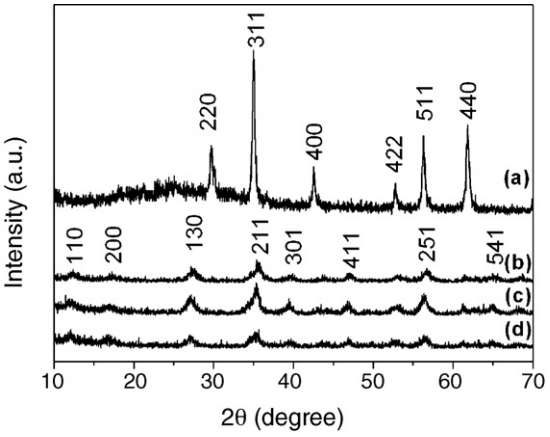

Fig. 3. XRD patterns of samples 5 (a), 6 (b), 7 (c) and 8 (d).

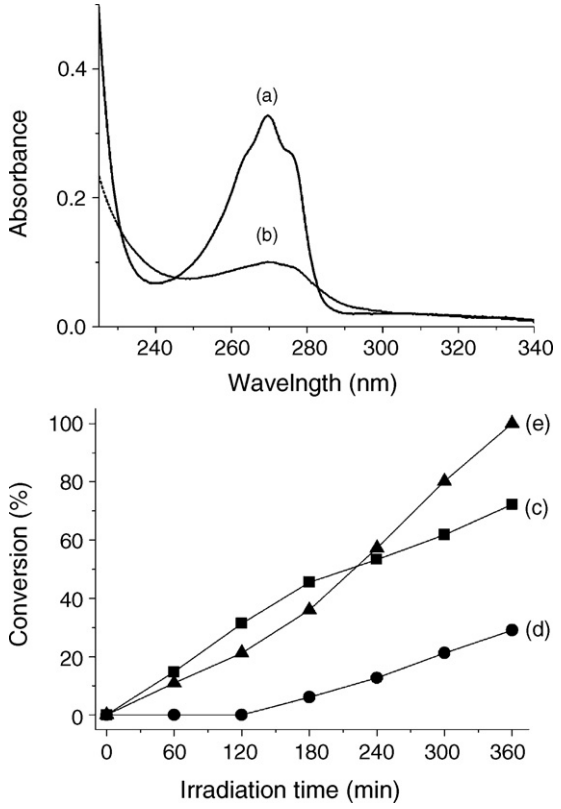

Fig. 4. (a) and (b) UV–vis absorption spectra of phenol solution in the presence of $ZnFe_2O_4$ nanoparticles (sample 1) before and after UV irradiation: (a) before UV irradiation, and (b) under UV irradiation for 360 min. (c)–(e) The degradation rate of phenol over different as-prepared photocatalysts: (c) $ZnFe_2O_4$ nanoparticles (sample 1), (d) in the absence of a photocatalyst, and (e) commercial TiO_2 (P25).

$ZnFe_2O_4$ has been successfully used as the heterogeneous catalyst for the oxidative dehydrogenation of *n*-butane to butene [28] and its use as a photocatalyst for phenol degradation has also been reported [8,29]. In order to evaluate the photocatalytic activity of as-prepared $ZnFe_2O_4$ nanoparticles (sample 1), the comparison experiments were performed. A suspension composed of 20 mg of $ZnFe_2O_4$ nanoparticles and 50 mL of phenol solution (20 mg L^{-1}) was placed in a 70 mL quartz tube and irradiated with UV light under continuous stirring. At different time intervals, analytical samples were withdrawn from the quartz tube and the phenol concentration was analyzed using a UV–vis spectrophotometer at a wavelength of 270 nm. Fig. 4a and b shows the UV–vis absorption spectra of phenol solution in the presence of $ZnFe_2O_4$ nanoparticles before and after UV irradiation for 360 min, from which one can see that the concentration of phenol decreases obviously after UV irradiation. Fig. 4c shows the degradation rate of phenol over $ZnFe_2O_4$ nanoparticles, from which one can see that the degradation percentage of phenol increases rapidly with increasing UV irradiation time, and reaches 73% in a time period of 360 min. The TOC measurement indicates that there is still 38% TOC remained after UV irradiation for 360 min. It has been reported that the products such as hydroquinone, catechol and benzoquinone were mainly detected during the UV irradiation [8]. However, the TOC measurement confirms that the $ZnFe_2O_4$ nanoparticles has an effective photocatalytic activity despite the formation of byproducts. Fig. 4d shows the degradation rate of phenol without adding the photocatalyst, from which one can see that phenol begins to degrade only after UV irradiation for 120 min and reaches only 29% in a time period of 360 min. It is obvious that as-prepared $ZnFe_2O_4$ nanoparticles exhibit a much better photocatalytic activity over phenol. We also investigated the photocatalytic activity of commercial TiO_2 (P25, Degussa, Germany) as a reference (Fig. 4e). One can see from Fig. 4e that the photocatalytic activity of $ZnFe_2O_4$ nanoparticles is higher than that of P25 before 180 min, but lower than that of P25 after 240 min. These results indicate that the $ZnFe_2O_4$ nanoparticles prepared by the MHIL method exhibit high photocatalytic activity over phenol.

4. Conclusions

We have successfully synthesized $ZnFe_2O_4$ nanoparticles via the MHIL method. The ionic liquid [BMIM][BF_4] and microwave heating temperature have significant influences on the crystal phase of the product. $ZnFe_2O_4$ nanoparticles can be obtained at appropriate dosage of [BMIM][BF_4]. The optimum microwave heating temperatures for the production of $ZnFe_2O_4$ are above 160 °C. The MHIL method is a simple, fast and energy-saving route for the production of $ZnFe_2O_4$ nanoparticles. And the $ZnFe_2O_4$ nanoparticles prepared by the MHIL method exhibit high photocatalytic activity for the degradation of phenol.

Acknowledgements

Financial support from the Program of Shanghai Subject Chief Scientist (07XD14031), the Fund for Nano-Science and Technology from Science and Technology Commission of Shanghai Municipality (0852nm05800), the National Natural Science Foundation of China (50772124, 50821004) is gratefully acknowledged.

References

[1] K. Raj, R. Moskowitz, Commercial applications of ferrofluids, J. Magn. Magn. Mater. 85 (1990) 233–245.
[2] A. Moser, K. Takano, D.T. Margulies, M. Albrecht, Y. Sonobe, Y. Ikeda, S. Sun, E.E. Fullerton, Magnetic recording: advancing into the future, J. Phys. D: Appl. Phys. 35 (2002) R157–R167.
[3] J.M. Bai, J.P. Wang, High-magnetic-moment core-shell-type FeCo–Au/Ag nanoparticles, Appl. Phys. Lett. 87 (2005) 152502.
[4] R.C. Che, L.M. Peng, X.F. Duan, Q. Che, X.L. Liang, Microwave absorption enhancement and complex permittivity and permeability of Fe encapsulated within carbon nanotubes, Adv. Mater. 16 (2004) 401–405.
[5] M. Sivakumar, T. Takami, H. Ikuta, A. Towata, K. Yasui, T. Tuziuti, T. Kozuka, D. Bhattacharya, Y. Iida, Fabrication of zinc ferrite nanocrystals by sonochemical emulsification and evaporation: observation of magnetization and its relaxation at low temperature, J. Phys. Chem. B 110 (2006) 15234–15243.
[6] L.D. Tung, V. Kolesnichenko, G. Caruntu, D. Caruntu, Annealing effects on the magnetic properties of nanocrystalline zinc ferrite, Physica B 319 (2002) 116–121.
[7] M. Wang, Z.H. Ai, L.Z. Zhang, Generalized preparation of porous nanocrystalline $ZnFe_2O_4$ superstructures from zinc ferrioxalate precursor and its superparamagnetic property, J. Phys. Chem. C 112 (2008) 13163–13170.
[8] M.A. Valenzuela, P. Bosch, J. Jimenez-Becerrill, O. Quiroz, A.I. Paez, Preparation, characterization and photocatalytic activity of ZnO, Fe_2O_3 and $ZnFe_2O_4$, J. Photochem. Photobiol. A: Chem. 148 (2002) 177–182.
[9] U. Steinike, K. Tkacova, Mechanochemistry of solids—real structure and reactivity, J. Mater. Synth. Process. 8 (2000) 197–203.
[10] S. Zhuiykov, T. Ono, N. Yamazoe, N. Miura, High-temperature NO_x sensors using zirconia solid electrolyte and zinc-family oxide sensing electrode, Solid State Ionics 152 (2002) 801–807.
[11] J.Z. Jiang, P. Wynn, S. Morup, T. Okada, F.J. Berry, Magnetic structure evolution in mechanically milled nanostructured $ZnFe_2O_4$ particles, Nanostruct. Mater. 12 (1999) 737–740.
[12] S.D. Shenoy, P.A. Joy, M.R. Anantharaman, Effect of mechanical milling on the structural, magnetic and dielectric properties of coprecipitated ultrafine zinc ferrite, J. Magn. Magn. Mater. 269 (2004) 217–226.
[13] H.H. Hamdeh, J.C. Ho, S.A. Oliver, R.J. Willey, G. Oliveri, G.J. Busca, Magnetic properties of partially-inverted zinc ferrite aerogel powders, J. Appl. Phys. 81 (1997) 1851–1857.
[14] S.H. Yu, T. Fujino, M. Yoshimura, Hydrothermal synthesis of $ZnFe_2O_4$ ultrafine particles with high magnetization, J. Magn. Magn. Mater. 256 (2003) 420–424.
[15] H.D. Xie, D.Z. Shen, X.Q. Wang, G.Q. Shen, Microwave hydrothermal synthesis and visible-light photocatalytic activity of Bi_2WO_6 nanoplates, Mater. Chem. Phys. 103 (2007) 334–339.
[16] X.L. Hu, J.C. Yu, J.M. Gong, Q. Li, G.S. Li, Alpha-Fe_2O_3 nanorings prepared by a microwave-assisted hydrothermal process and their sensing properties, Adv. Mater. 19 (2007) 2324–2329.

[17] X.L. Hu, J.C. Yu, Continuous aspect-ratio tuning and fine shape control of monodisperse alpha-Fe_2O_3 nanocrystals by a programmed microwave-hydrothermal method, Adv. Funct. Mater. 18 (2008) 880–887.
[18] Y.J. Zhu, W.W. Wang, R.J. Qi, X.L. Hu, Microwave-assisted synthesis of single-crystalline tellurium nanorods and nanowires in ionic liquids, Angew. Chem. Int. Ed. 43 (2004) 1410–1414.
[19] K.L. Ding, Z.J. Miao, Z.M. Liu, Z.F. Zhang, B.X. Han, G.M. An, S.D. Miao, Y. Xie, Facile synthesis of high quality TiO_2 nanocrystals in ionic liquid via a microwave-assisted process, J. Am. Chem. Soc. 129 (2007) 6362–6363.
[20] Y. Jiang, Y.J. Zhu, G.F. Cheng, Synthesis of Bi_2Se_3 nanosheets by microwave heating using an ionic liquid, Cryst. Growth Des. 6 (2006) 2174–2176.
[21] W.W. Wang, Y.J. Zhu, Synthesis of $PbCrO_4$ and Pb_2CrO_5 rods via a microwave-assisted ionic liquid method, Cryst. Growth Des. 5 (2005) 505–507.
[22] O.M. Alfano, D. Bahnemann, A.E. Cassano, R. Dillret, R. Goslich, Photocatalysis in water environments using artificial and solar light, Catal. Today 58 (2000) 199–230.
[23] D. Tryk, A. Fujishima, K. Honda, Recent topics in photoelectrochemistry: achievements and future prospects, Electrochim. Acta 45 (2000) 2363–2376.
[24] D.S. Bhatkhande, V.G. Pangarkar, A. Beenackers, Photocatalytic degradation for environmental applications–a review, J. Chem. Technol. Biotechnol. 77 (2002) 102–116.
[25] S.K. Pardeshi, A.B. Patil, A simple route for photocatalytic degradation of phenol in aqueous zinc oxide suspension using solar energy, Solar Energy 82 (2008) 700–705.
[26] R.L. Autenrieth, J.S. Bonner, A. Akgerman, E.M. Mccreary, Biodegradation of phenolic wastes, J. Hazard. Mater. 28 (1991) 29–53.
[27] C.H. Chiou, C.Y. Wu, R.S. Juang, Influence of operating parameters on photo-catalytic degradation of phenol in UV/TiO_2 process, Chem. Eng. J. 139 (2008) 322–329.
[28] J. Peral, X. Domenech, D.F. Ollis, Heterogeneous photocatalysis for purification, decontamination and deodorization of air, J. Chem. Technol. Biotechnol. 70 (1997) 117–140.
[29] W.Q. Meng, F. Li, D.G. Evans, X. Duan, Photocatalytic activity of highly porous zinc ferrite prepared from a zinc–iron(III)-sulfate layered double hydroxide precursor, J. Porous Mater. 11 (2004) 97–105.